Physics in Medicine & Biology

IPEM Institute of Physics and Engineering in Medicine

PAPER

Simulation of light transport in scintillators based on 3D characterization of crystal surfaces

To cite this article: Emilie Roncali and Simon R Cherry 2013 *Phys. Med. Biol.* **58** 2185

View the article online for updates and enhancements.

Related content

- An integrated model of scintillator-reflector properties for advanced simulations of optical transport
Emilie Roncali, Mariele Stockhoff and Simon R Cherry
- Predicting the timing properties of phosphor-coated scintillators using Monte Carlo light transport simulation
Emilie Roncali, Jeffrey P Schmall, Varsha Viswanath et al.
- Advanced optical simulation of scintillation detectors in GATE V8.0: first implementation of a reflectance model based on measured data
Mariele Stockhoff, Sebastien Jan, Albertine Dubois et al.

Recent citations

- Modelling the transport of optical photons in scintillation detectors for diagnostic and radiotherapy imaging
Emilie Roncali *et al*
- Simulation of scintillation light output in LYSO scintillators through a full factorial design
Francis Loignon-Houle *et al*
- Advanced optical simulation of scintillation detectors in GATE V8.0: first implementation of a reflectance model based on measured data
Mariele Stockhoff *et al*

Quantify 3D Geometric Distortion in MR Images
Verify the accuracy of target delineation and treatment efficacy for MRgRT
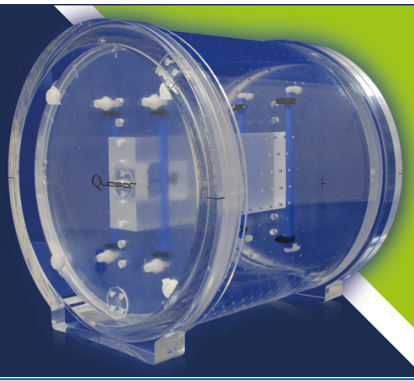
Watch Video
modusQA
Accuracy. Confidence.™

This content was downloaded from IP address 115.27.204.51 on 23/12/2017 at 13:35

IOP Publishing Physics in Medicine and Biology

Phys. Med. Biol. **58** (2013) 2185–2198 doi:10.1088/0031-9155/58/7/2185

Simulation of light transport in scintillators based on 3D characterization of crystal surfaces

Emilie Roncali and Simon R Cherry

Department of Biomedical Engineering, University of California Davis, 1 Shields Avenue, Davis, CA 95616, USA

E-mail: eroncali@ucdavis.edu

Received 13 December 2012
Published 11 March 2013
Online at stacks.iop.org/PMB/58/2185

Abstract

In the development of positron emission tomography (PET) detectors, understanding and optimizing scintillator light collection is critical for achieving high performance, particularly when the design incorporates depth-of-interaction (DOI) encoding or time-of-flight information. Monte-Carlo simulations play an important role in guiding research in detector designs and popular software such as GATE now include models of light transport in scintillators. Although current simulation toolkits are able to provide accurate models of perfectly polished surfaces, they do not successfully predict light output for other surface finishes, for example those often used in DOI-encoding detectors. The lack of accuracy of those models mainly originates from a simplified description of rough surfaces as an ensemble of micro-facets determined by the distribution of their normal, typically a Gaussian distribution. The user can specify the standard deviation of this distribution, but this parameter does not provide a full description of the surface reflectance properties. We propose a different approach based on 3D measurements of the surface using atomic force microscopy. Polished and rough (unpolished) crystals were scanned to compute the surface reflectance properties. The angular distributions of reflectance and reflected rays were computed and stored in look-up tables (LUTs). The LUTs account for the effect of incidence angle and were integrated in a light transport model. Crystals of different sizes were simulated with and without reflector. The simulated maximum light output and the light output as a function of DOI showed very good agreement with experimental characterization of the crystals, indicating that our approach provides an accurate model of polished and rough surfaces and could be used to predict light collection in scintillators. This model is based on a true 3D representation of the surface, makes no assumption about the surface and provides insight on the optical behaviour of rough crystals that can play a critical role in optimizing the design of PET detectors. This approach is also compatible with existing simulation toolkits and next steps include the implementation in GATE.

(Some figures may appear in colour only in the online journal)

 © 2013 Institute of Physics and Engineering in Medicine Printed in the UK & the USA

1. Introduction

In the development of positron emission tomography (PET) detectors, understanding and optimizing scintillator light collection is critical for achieving high performance, particularly when the detector design incorporates depth-of-interaction (DOI) encoding or time-of-flight (TOF) information (Spanoudaki and Levin, 2011). Among the various schemes providing DOI information, solutions including dual-ended readout of the scintillator (Moses and Derenzo 1994), light sharing between crystals (Miyaoka *et al* 1998, Yang *et al* 2009), phosphor-coated crystals (Du *et al* 2009), have proven to work best with unpolished crystals that have a rough surface (Shao *et al* 2002, Yang *et al* 2006).

Optical Monte-Carlo simulations allow for the modelling of light transport in scintillators together with light collection by photodetectors, and have been extensively used to study PET detector performance. Various software such as DETECT (Knoll *et al* 1988), (Cayouette *et al* 2003), GEANT4 (Agostinelli *et al* 2003), GATE (Jan *et al* 2004) or Litrani (Gentit 2002), have been developed to perform such tasks. Optical design software such as ZEMAX may also be used (Bauer *et al* 2009). Those programs typically generate scintillation photons when a gamma ray interacts with the crystal; each of these scintillation photons is tracked individually until it either reaches the photodetector surface or escapes the crystal. The light transport in the crystal is dependent on the crystal geometry, the bulk absorption and scattering of the material, and the surface treatment of the crystal faces. While the bulk properties of the scintillator are known for a given material, the roughness of the crystal surface is very dependent on the cutting tools and processes used, as well as the effects of any additional surface treatments (polishing, etching, etc . . .). In the simulation toolkits mentioned above, surfaces are described by an ensemble of micro-facets characterized by the orientation of their normal vectors. Earlier versions of DETECT assumed that for a rough surface, the micro-facet normals followed a Lambertian distribution, whereas later versions are based on the UNIFIED model (Nayar *et al* 1991, Levin and Moisan 1996). In the UNIFIED model, implemented in the latest versions of GEANT4 and GATE, the micro-facets are assumed to follow a Gaussian distribution whose standard deviation can be defined by the user and four different probability distributions describe the reflection properties of a surface. For each new type of surface, the user needs to specify the standard deviation of the Gaussian distribution (i.e. roughness of the surface) and also weight the contribution of each reflection type, adding several degrees of freedom to the definition of the behaviour of the surface. While these simulation tools perform well when modelling polished crystals where surfaces behave very much like ideal specular reflectors (van der Laan *et al* 2010), they present important shortcomings at accurately predicting light output of etched or rough crystals, even when using measured surface parameters (Bea *et al* 1994, Janecek and Moses 2010). Bauer *et al* (2009) simulated etched crystals using a standard deviation 0.3 rad in the Gaussian distribution of micro-facets, but needed to add an air layer to obtain a good agreement with measurements. The reasons for inaccuracy in modelling rough surfaces are that (1) the surface is described only by the orientation of micro-facets, height is not included, and (2) the model assumes that the reflectance properties of the surface are independent of the incidence angle, which is not consistent with data reported by Janecek and Moses (2009). One way to characterize the surface roughness is to measure line profiles using a stylus probe (Levin and Moisan 1996) but the information is 2D only and the resolution is limited by the diameter of the stylus probe. Janecek and Moses (2010) proposed to use measured reflectance data and obtained very good agreement with experimental results. Their model is based on the experimental characterization of the angular reflection distribution of scintillators (50.8 mm diameter crystal hemispheres), using an array of 36 PIN photodiodes arranged in a half ring geometry. Though the use of measured reflectance data allows for a

very accurate prediction of the light collection, it requires a very specific experimental setup together with large and expensive hemispherical test samples. This approach also does not allow the measurement of the reflectance of already cut crystals.

We propose a different approach based on 3D measurements of the crystal surfaces. Surface samples were scanned with 3D atomic force microscopy (AFM) and used to compute reflectance properties of the crystal surfaces. We developed an algorithm to compute the angular distribution of reflectance and reflected rays at various incidence angles for each surface sample. The *angular distribution of reflectance* contains the probabilities that rays hitting the surface at different incident angles are reflected, whereas the *angular distribution of reflected rays* contains the distribution of reflection directions for various incidence angles. These data were stored in look-up tables (LUTs) and then used during modelling of scintillation photon transport in the volume of the crystal using a custom simulation code that enables the generation of gamma interactions and optical tracking of each of the scintillation photons. Each time a photon reaches the surface of the crystal with a certain angle of incidence, the angular distribution of reflectance LUT is used to determine whether the photon is reflected and if it is, a random direction of reflection is selected from the angular distribution of reflected rays LUT for this specific incident angle. All photons collected by the photodetector are stored with their emission time and wavelength. This method is comparable to that of Janecek and Moses (2010) as it is based on LUTs obtained from measured data, accounts for the effect of the incidence angle and does not rely on a theoretical model of the surface. However it has the advantage of being compatible with any geometry of crystal, as opposed to the reflectance measurement setup previously described. In addition, in this work the characterization of the crystals was performed with a standard AFM that provides a true representation of the crystal surface with very high spatial resolution ($\sim$100 nm), and can be found in many research facilities.

To validate our method, various samples of rough and polished crystals were scanned using AFM. The angular distribution of reflectance and reflected rays were computed for each surface and incorporated in our light transport model. Different crystal sizes and surface treatment were simulated with and without reflector. Similarly, experimental studies were performed on crystals with different sizes and roughness, with and without reflector. The characterization of the light collection was carried out using two approaches. Firstly, surface roughness controls the reflection of photons at the crystal faces, and thus contributes to the light loss along the crystal length. The light output (light collected at the exit face of the crystal) is therefore depth-dependent and was studied as a function of DOI for all configurations. Secondly, the light collection was characterized by looking at the maximum light output, typically obtained when the crystal is irradiated close the photodetector face (Huber *et al* 1999). Light collection obtained from these simulations was compared to experimental values and to simulations performed with the UNIFIED model.

2. Materials and methods

2.1. Characterization of the crystal surfaces

2.1.1. Topography of the surface using AFM. $2 \times 2 \times 20$ mm^3 lutetium oxyorthosilicate (LSO) crystals were characterized using AFM. Two crystals had all sides coarse ground finished (saw cut then polished with a 30 μm grit paper) and one end polished while another crystal had all faces mechanically polished. The coarse ground finish crystals will be referred as 'rough crystals' in the rest of this paper. One side face of each crystal was characterized in two different locations using an Asylum MFP-3D atomic force microscope (Asylum Research, Santa Barbara CA). 90 μm $\times$ 90 μm areas were scanned in contact mode with a silicon micro cantilever (AC160, Olympus Corp. Japan), a speed of 45 μm s^{-1} and a pixel size of 0.175 μm.

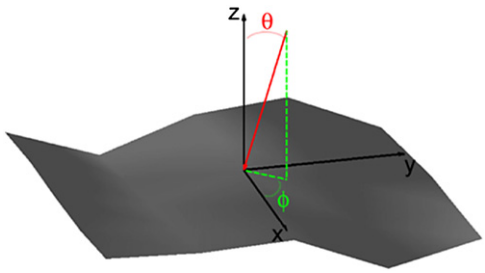

Figure 1. In red: incident ray, defined by angles (θ, ϕ). In green: projection of the incident ray in **xy** plane. The incidence angle θ is defined with respect to the z axis and the azimuthal angle ϕ is defined with respect to the x axis.

Oscillations from the tip of the AFM lever were filtered using a weighted local regression smoothing. One surface sample was taken on one face of the polished crystal and a second sample was taken from a different face. All the four rough surfaces and two polished surfaces were then used to compute reflectance properties and LUTs.

2.1.2. Computing the angular distribution of reflectance and reflected rays. The goal of this calculation was two-fold: (1) compute the probability for a photon arriving on the surface at a given incidence angle to be reflected; (2) compute the angular distribution of reflected rays. The angular distribution of reflectance and reflected rays were calculated simultaneously for incidence angles θ varying between 0 (normal incidence) and 90° with a sampling of 2.25°.

For each incidence angle θ, the measured surface was randomly illuminated by a simulated collimated beam of ∼2000 incident photons whose principal direction was defined by θ and ϕ (figure 1). Each photon was tracked to its interaction point on the surface and the orientation of the surface at that point with respect to the photon direction determined. Fresnel equations were used to compute the probability for this photon to be reflected by the surface. This probability depends on the incidence angle, the local surface normal, the refractive index of the incident medium (here the crystal) and the refractive index of the external medium. The index of refraction of LSO was set at 1.82 while the external medium was considered to be air (reflector not attached to the surface) or optical grease (index of refraction ∼1.5) for the face in contact with the photodetector entrance window. When a photon was reflected, it underwent a specular reflection with respect to the local normal of the surface. The photon then moved away from the surface and was considered to re-enter the incident medium if it did not interact with the surface again. In the case of multiple reflections, the photon was tested for reflection using the same protocol. For a given incident angle θ, the collimated beam was then rotated with respected to the z axis by varying the azimuthal angle ϕ between 0 and 360° in steps of 9° and ∼2000 incident photons were projected onto the surface once again. This increases the sampling of the surface at various incidence angles and accounts for any directionality in the surface finish. Finally, for each incident angle θ, all azimuthal angles ϕ were combined and the reflectance was computed as the ratio between the number of reflected photons and the number of incident photons. The angular distribution of reflectance and all reflected rays as function of incidence angle were saved and stored in LUTs.

2.2. Simulation of light collection with the LUTs for different crystal geometries

Our Monte-Carlo simulation code was then used to model gamma interactions occurring at different depths in the scintillator and to generate light pulses to be recorded by a

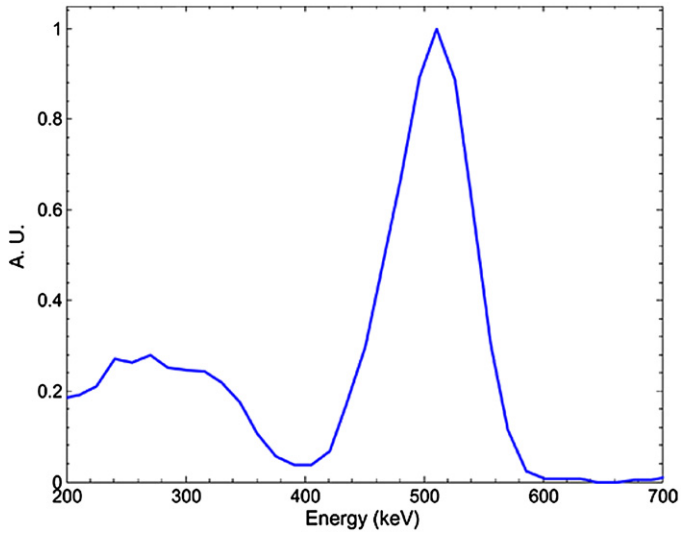

Figure 2. Energy distribution used to generate gamma interactions in the crystal.

photodetector. In this work, all parameters were chosen to simulate a LSO crystal as employed in the experimental setup used for validation. The bulk LSO material was modelled with an index of refraction of 1.82, an absorption length of 300 mm and a scattering length of 256 mm (Rothfuss *et al* 2004). For each gamma interaction, the energy of the interaction was randomly selected following a distribution derived from an energy spectrum measured with a $2 \times 2 \times 20$ mm^3 LSO polished (figure 2).

The corresponding number of scintillation photons was then calculated assuming a light yield of 25 photons/keV (Moszynski *et al* 1997). The measured energy distribution accounts for the statistical variation introduced by the light yield of the scintillator and the quantum efficiency (QE) of the detector. We considered only photoelectric effect and Compton scattering. For each gamma interaction visible photons were emitted isotropically, creating a light pulse. The fate of these individual photons was tracked. Appropriate wavelength and time of emission for each photon were assigned based on scintillator properties. Scintillators produce light pulses with an exponential decay (∼40 ns for LSO) (Melcher and Schweitzer 1992), thus the emission times assigned to individual photons followed an exponential distribution with a 40 ns decay. Scintillator rise time was ignored. The emission spectrum of LSO was measured on crystals from the same bulk material as that used for experiments with time resolved fluorescence spectroscopy (TRFS) (Yang *et al* 2009). The wavelength of the photons generated was selected by randomly sampling the measured emission spectrum.

On encountering the edges of the scintillator, photons may be reflected or transmitted (figure 3(a)). If a photon reaches the scintillator/photodetector boundary, it may be transmitted and detected, or reflected. A fraction of photons also escapes the crystal. The photodetector was modelled by its QE spectrum. For the simulations presented here, the QE of a Hamamatsu R6231 PMT was used. The size of the photodetector was set to match the size of the crystal. The reflection properties of the crystal surfaces were modelled using the LUTs computed from the AFM surface measurements. One end of the crystal was modelled as a polished surface in contact with optical grease (index of refraction 1.5) whereas all the other faces were modelled in contact with air (both in the case of an external reflector such as Teflon tape and no reflector) and either polished or rough depending on the type of crystal simulated. In some simulations, an external diffuse reflector was modelled by its reflection coefficient of 0.97, corresponding

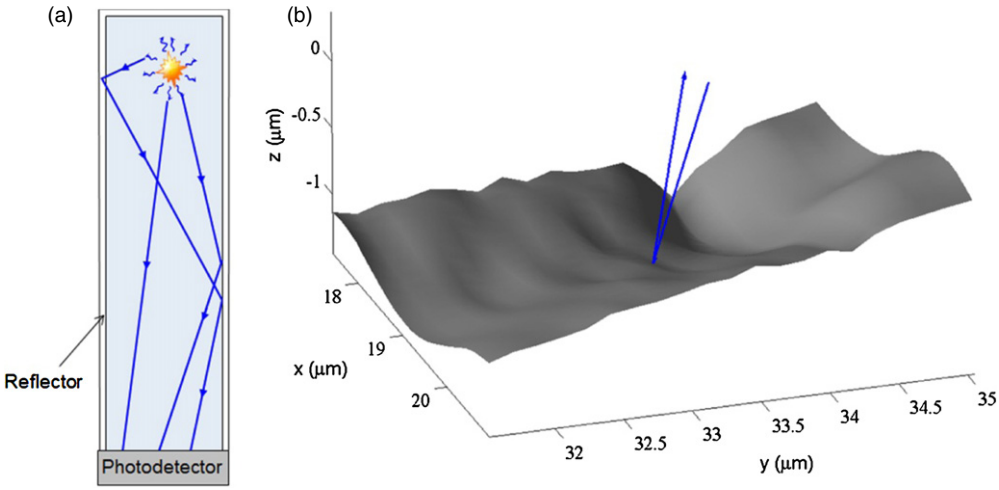

Figure 3. (a) Schematic representation (not to scale) of scintillation photons in a crystal covered by an external reflector. (b) When hitting the surface, rays (in blue) may be reflected.

to a diffuse reflector such as Teflon tape. This reflector was assumed to be Lambertian and so the direction of reflected photons followed a Lambertian distribution. Photons were refracted when they re-entered the crystal. Arrival times and wavelengths of detected photons were recorded and used to generate simulated light pulses and spectra.

Different configurations were investigated: $2 \times 2 \times 20$ mm^3 and $5 \times 5 \times 20$ mm^3 'rough' crystals (ground finish surfaces) were simulated without and with reflector using the LUTs computed from the 'rough' surface samples measured on such crystals. $2 \times 2 \times 20$ mm^3 LSO polished crystals were also simulated. For each crystal, 500 light pulses were generated in 1.5 mm bins at five different depths every 4 mm starting 2 mm away from the photodetector face that is at 0 mm. At each depth, the energies were histogrammed and the photopeak positions were extracted from the energy spectra to characterize the light output variation with depth. The maximum light output was defined as the photopeak position at the irradiation depth closest to the photodetector, 2 mm. All maximum light output values were normalized by the maximum light output of the polished crystal with reflector (expected to be the highest).

2.3. Simulation using the 'UNIFIED' model for different crystal geometries

Simulations were also carried out using the Monte-Carlo simulation code described in section 2.2 but with a reflection model similar to the UNIFIED model described in Levin and Moisan 1996. Crystal surfaces were described by an ensemble of micro-facets characterized by the orientation of their normal vectors. The normal vectors are assumed to follow a Gaussian distribution whose standard deviation is defined by the surface roughness and four different probability distributions (specular spike for reflections by the average surface, specular lobe for reflections by a micro-facet, backscatter to reflect photons towards incident direction and Lambertian). The surface roughness was estimated from our topographical measurements with AFM to be ∼18 degrees for the rough crystals and 1.2° for the polished crystals (see section 3.2.1). As prescribed by Levin and Moisan 1996, the specular lobe probability was set at 1 while the other probabilities were set at 0. All other parameters were identical to the simulations with the LUTs.

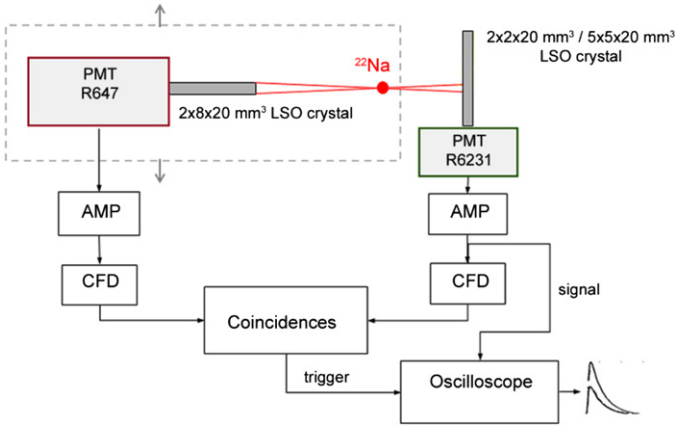

Figure 4. Experimental setup.

2.4. Light collection measurements

Crystals were coupled to a single-channel photomultiplier tube (Hamamatsu R6231) using optical grease (BC-630, Bicron). The detector, composed of the crystal of interest coupled to the photomultiplier tube (PMT), was positioned in coincidence with a collimating detector consisting of a $2 \times 8 \times 20$ mm^3 block of LSO coupled to a single channel PMT (Hamamatsu R647). As shown in figure 4, the orientation of the crystal in the collimating detector was chosen such that it was irradiated face-on, whereas the crystal to be studied was irradiated from the side by a 0.5 mm ^{22}Na point source of activity 3.7 MBq. The collimating detector together with the source was translated to irradiate the crystal of interest along its length at five different depths every 4 mm starting 2 mm away from the photodetector face by using electronic coincidence to select events. The 0 depth is defined to be at the crystal face in contact with the PMT. The estimated width of the collimating beam at the crystal was 1.5 mm. The signal from the R6231 PMT was passed through a fast amplifier (NIM Model 778, Philips Scientific, Ramsey, NJ) and recorded by an oscilloscope (Lecroy WavePro 7100). Signals from both PMTs were sent to constant fraction discriminators (CFD TC 453, Oxford Instruments Inc., Oak Ridge TN) and CFD signals were used to identify coincidence events with a quad-four fold logic unit (Model 756, Philips Scientific, Ramsey, NJ). The coincidence events were used to trigger the acquisition of $\sim$1000 individual pulses at each depth with a sampling interval of 0.1 ns for each pulse (sampling rate 10 GHz). Pulses were downsampled to a 1 GHz sampling rate before being processed.

Four $2 \times 2 \times 20$ mm^3, four $5 \times 5 \times 20$ mm^3 rough crystals and two $2 \times 2 \times 20$ mm^3 mechanically polished crystals were measured with and without reflector. Maximum light outputs were normalized by the values acquired with $2 \times 2 \times 20$ mm^3 polished crystals with reflector.

3. Results

3.1. Characterization of the crystal surfaces with AFM

Figure 5(a) shows that the mechanically polished LSO surface appears flat and still reveals a few shallow scratches resulting from the polishing operation. A close up of the yellow region drawn on figure 5(a) (figure 5(b), not to scale) shows that the surface height ranges from ~ -0.05 μm

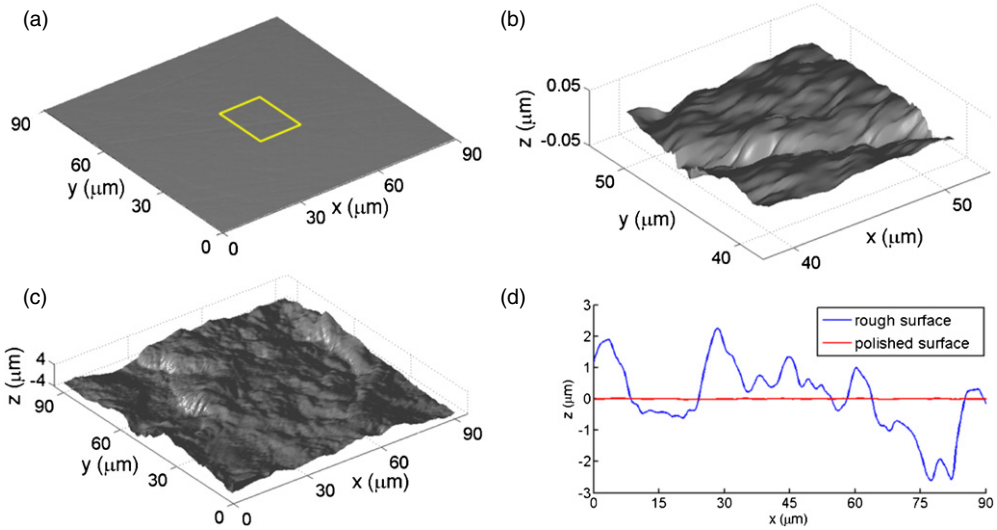

Figure 5. (a) 3D view of a 90 μm $\times$ 90 μm polished surface, using AFM. (b) 3D view of the area within the yellow square with height scale magnified. Height ranges from ~ -0.05 μm to 0.05 μm. (c) 3D view of a 90 μm $\times$ 90 μm rough surface on same scale as (a). Height ranges from ~ -3 μm to 3 μm. (d) Line profiles taken at $y = 45$ μm from both surfaces.

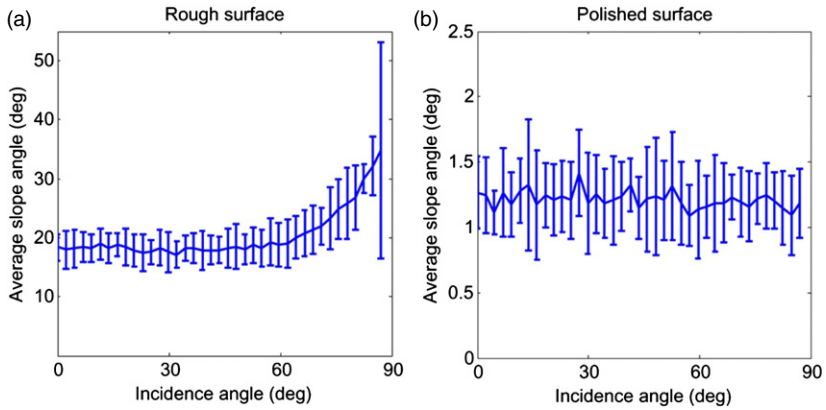

Figure 6. (a) Average slope versus incidence angle for a rough surface. (b) Average slope versus incidence angle for a polished surface.

to 0.05 μm, the deepest area being in the scratch. Rough LSO crystal surfaces scanned with AFM (figure 5(c)) exhibit greater roughness, with height varying between ~ -3 μm and 3 μm. Numerous small faces with different orientations are visible. The comparison of line profiles measured on rough and polished surfaces along the x axis at $y = 45$ μm (figure 5(d)) illustrates the different range in height variation.

3.2. Reflectance properties

3.2.1. Surface orientation as a function of incidence angle. For each photon hitting the surface, the local slope of the surface was calculated. Values were averaged for each incidence angle and plotted against that angle for four rough surfaces (figure 6(a) shows the average of

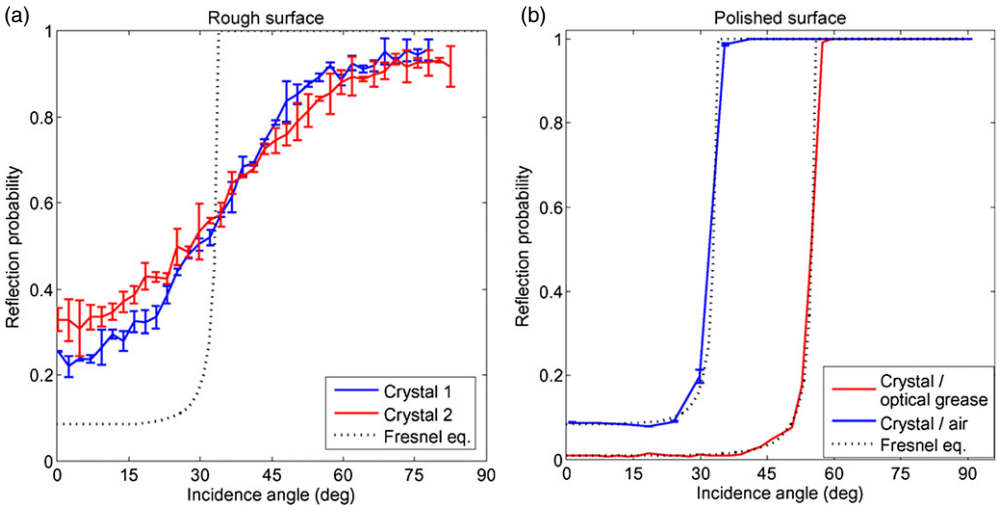

Figure 7. (a) Reflectance curves for rough surface. (b) Reflectance curves for polished surface. Black dotted lines show Fresnel equations for interface crystal/air (33.3°) and crystal/optical grease (55.5°).

the four surfaces with minimum and maximum values). The average slope has a baseline at ∼18° and increases with the incidence angle up to 35°. This indicates that there is a shadowing effect and thus the photons will encounter different slopes depending on their incidence angle. This clearly affects the distribution of reflected rays and may tend to enhance backscattering at high incidence: photons interacting with the surface at high incidence will encounter faces with a steeper slope that will reflect the photons more towards their incoming direction than faces with gentler slope. In order to accurately model a rough surface, this dependence should be taken into account when computing the reflectance properties. On the contrary, the polished surface shows no dependence on the incidence angle and has an average slope angle of 1.25° (figure 6(b)).

3.2.2. Reflectance probability. Results of the angular distribution of the reflectance are presented in figures 7(a) and (b) (rough and polished surface, respectively). Two surface samples were taken on each rough crystal and each curve on figure 7(a) corresponds to the average value of the two samples, with bars indicating the values corresponding to each sample. The two crystals show similar behaviour, which indicates that a small sample of a crystal side (90 μm $\times$ 90 μm) accurately represents the whole surface roughness. Both curves show a steep increase around 33° that corresponds to the critical angle for an LSO/air interface. The reflectance computed from Fresnel equations for unpolarized light crossing an LSO/air interface (black dotted curve) also shows an expected steep increase at the critical angle followed by unity reflection probability due to total internal reflection. By comparing the reflectance curves computed for the rough surfaces to the theoretical reflectance, we observe that the roughness of the surface tends to increase the reflectance at low incidence angles, smoothes the transition to the total internal reflection at high incidence angles and lowers the reflectance in this range. Reflectance curves obtained for a polished surface in contact with air or optical grease are shown on figure 7(b) together with the reflectance computed from the Fresnel equation for LSO/air and LSO/optical grease interfaces (dotted lines). In both cases an almost a perfect overlap between the theoretical and computed reflectance curves is observed, indicating that a mechanically polished surface acts as an ideal flat surface.

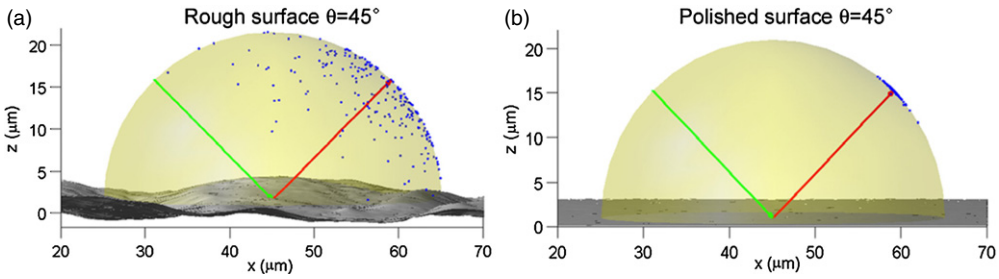

Figure 8. Example of reflected rays for an incidence angle of 45° for (a) a rough surface and (b) a polished surface. Incident ray is shown in green. Specular reflection of the green ray by a flat surface is shown in red. Blue points show the distribution of interaction points of individual reflected rays on a hemispherical surface for the two different surfaces.

3.2.3. Ray distribution. For photons at each incidence angle, the angular distribution of the reflectance and the angular distribution of reflected rays were computed. For a given incident angle, the rough surfaces tend to disperse the reflected rays compared to a flat surface. An example of reflected rays for incident rays hitting a rough surface at 45° is shown in figure 8(a). While incident rays (in green) would be specularly reflected by an ideal flat surface along the red direction, the rough surface distributes the reflected rays into a large solid angle, due to the many different slopes encountered by the photons. On the contrary, a polished surface behaves very much like a specular reflector: almost all the reflected rays are confined in a narrow solid angle centred on the specular reflected ray (figure 8(b)). This illustrates the importance of proper assessment of the reflection distribution to be used when modelling light reflection on the crystal sides. The fate of photons interacting with the sides is not only determined by the reflection probability but also by the direction of the reflected rays. This will change the number of reflections that photons undergo on their way to the photodetector face and therefore the ultimate signal detected.

3.3. Effect of depth on light output

Results of light transport simulation using reflectance LUTs are presented together with experimental characterization, and results obtained with the UNIFIED model. Figure 9(a) shows the comparison between LUT-simulated data (in blue), experimental data (in red) without reflector. A clear and different depth-dependence is observed for rough crystals of the two sizes; no significant depth dependence is observed for polished crystals. For each crystal size, LUT-simulated values were averaged for the 4 surface samples used to model the surface. All LUT-simulated data show very little variation (see error bars corresponding to the standard deviation), which indicates that the samples used here were sufficient to provide a representative description of the crystal surfaces. Experimental data acquired with identical crystals of each size were averaged as well. This figure shows a very good agreement between experimental and LUT-simulated data, for all crystal sizes and roughness. This indicates that the LUTs used in the simulations provide an accurate model of the surface reflectance properties. In contrast, the UNIFIED model shows a weaker depth-dependence for rough crystals of both sizes and hence overestimates the light output when the DOI increases. As expected, the UNIFIED model has very good agreement with experimental data for polished crystals.

Results with a reflector on the crystal sides also show very good agreement between LUT simulations and experiments (figure 9(b)), especially for $2 \times 2 \times 20$ mm^3 crystals.

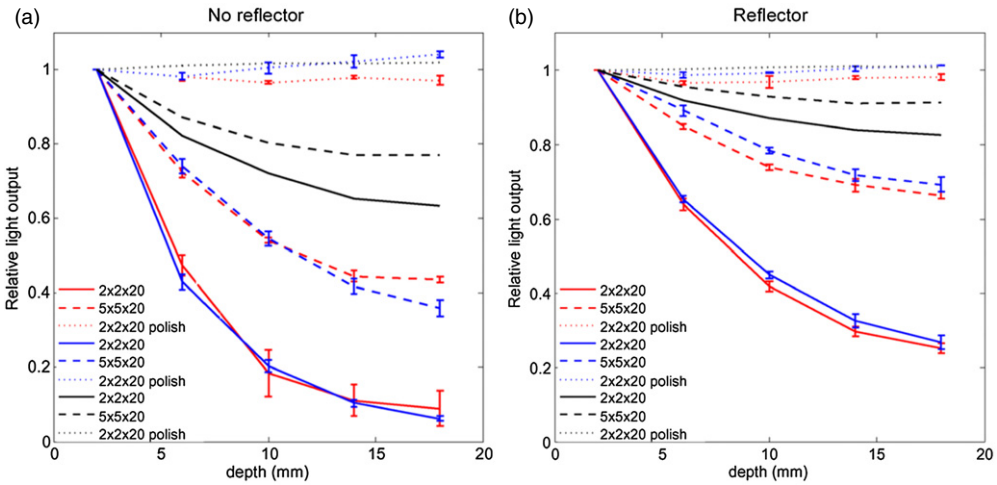

Figure 9. (a) Relative light output versus depth, without reflector. (b) Relative light output with reflector $R = 0.97$. For rough and polished crystals of different size, experimental results are shown in red, LUT-simulations in blue, and UNIFIED results in black.

Small discrepancies between simulation and experiments may arise from imperfect model of the reflector. The reflection coefficient used for the Teflon tape is consistent with previous work (Janecek and Moses 2010, van der Laan *et al* 2010). In addition we found very good agreement between the energy resolution for experimental and LUT-simulated results for the $2 \times 2 \times 20$ mm^3 rough crystals (24% and 22%, spectra not shown here). The UNIFIED model with reflector shows good agreement with experimental data for polished crystals but underestimates the depth-dependence for rough crystals of both sizes, as observed previously in the results without reflector.

3.4. Maximum light output

Secondly, maximum light outputs were studied for all configurations (figure 10). In the LUT-simulations, ∼1650 photons per event were collected by the photodetector when irradiating at 2 mm from the photodetector, which is consistent with results reported for LSO crystals of similar size coupled to PMT with similar QE (Huber *et al* 1999, Bauer *et al* 2009). For LUT-simulated data, bar plots show the average of the four samples for rough crystals and two samples for polished crystals. Error bars indicate the minimum and maximum values obtained between the samples and showed very little variation, which confirms the robustness of the model as previously observed when studying the light output as a function of DOI. For experimental data, bar plots are the average values of all characterized crystals (four for rough crystals and two for polished crystals). Error bars indicate the minimum and maximum values between crystals. A greater error is observed with experimental data, which can be attributed to variation in the coupling of the crystals to the PMT via optical grease. When comparing LUT- simulated and experimental values obtained without reflector, there is a very good agreement for the $2 \times 2 \times 20$ mm^3 rough and polished crystals and a larger difference for the $5 \times 5 \times 20$ mm^3 crystals. This may be explained by the fact that the $2 \times 2 \times 20$ mm^3 crystals were used for both the surface 3D scans and experimental measurements of light levels. Maximum light outputs obtained with the UNIFIED model (in black) for $2 \times 2 \times 20$ mm^3 rough crystals overestimated the light output (+38%) compared

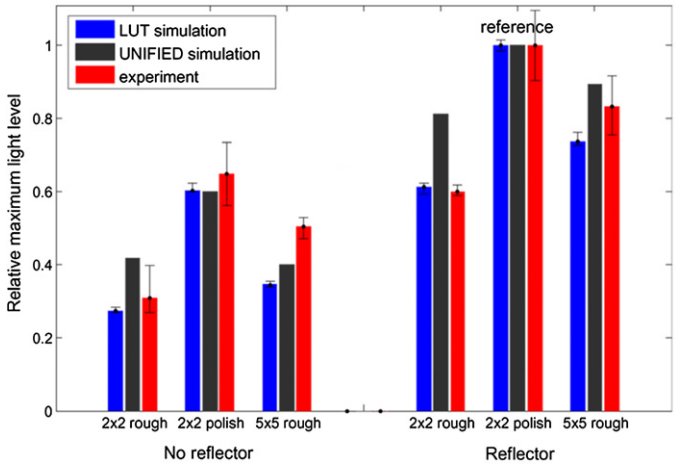

Figure 10. Relative maximum light output for experimental and simulated data. Values were normalized by the value obtained from a polished 2 × 2 × 20 mm^3 crystal with reflector. Experimental results are shown in red, LUT-simulations in blue, and UNIFIED results in black.

with experimental results. This model showed better agreement for the 5 × 5 × 20 mm^3 rough crystal (+20%). This indicates that the UNIFIED model performs better when photons undergo a small number of reflections (such as in crystals with larger aspect ratio).

LUT-simulations with reflector show very good agreement for all crystal sizes (∼10% difference for 5 × 5 × 20 mm^3 crystals and less than 2% for 2 × 2 × 20 mm^3 crystals). The UNIFIED model overestimated the maximum light output for both rough crystals (∼10% for 5 × 5 × 20 mm^3 crystals and ∼30 % for 2 × 2 × 20 mm^3 crystals).

4. Discussion

The goal of this work was to develop an accurate model of surfaces in order to simulate light transport in scintillation crystals. The proposed approach is based on the computation of reflectance properties of real crystal surfaces scanned with a 3D atomic force microscope, combined with a model of light reflection on the crystal sides and photon tracking. The model led to very good agreement between simulation and experimental characterization with no a priori assumption about the surfaces. Our simulations showed no increase and even a reduction in computation time in certain configurations (−10% for the 2 × 2 × 20 mm^3 without reflector) compared to the UNIFED model, which is important as computational burden of Monte-Carlo simulations is already high. We thoroughly studied the reflectance properties of the surfaces and observed a clear effect of the incidence angle, which is consistent with the work from Janecek and Moses (2010) and emphasizes the fact that standard models not accounting for the incidence angle will likely be less accurate.

The angular distribution of reflectance angles computed for rough surfaces showed a slight variation between crystals from the same batch (same manufacturing conditions). However, no significant variation in computed light levels was observed. Larger slopes (steeper faces) increase the chance of multiple reflections and these are processed by our model because it is based on a real 3D characterization of the surface that includes not only the slope of the surface but also the height of the facets.

Our approach was validated on a small number of crystals issued from the same manufacturing batch available in our laboratory. Future studies will include a more detailed

characterization of crystal surfaces to study the robustness of our method and the ability of the model to predict light output for a specific crystal using a surface sample measured on a different crystal. This type of study will also allow us to investigate the effect of different surface treatments, the variability across samples and have a better understanding of the reflectance properties of rough and etched crystal surfaces. In the work presented here, only LSO crystals were simulated and studied experimentally. To study the ability of the proposed technique to model scintillator the optical behaviour of various materials, other scintillators will be investigated. Another critical point in modelling light transport in scintillators is the reflector. The work presented here was based on a diffuse detector not attached to the surface. Other reflectors types could be modelled and reflectance properties of a rough surface with a glued specular or diffuse reflector could be computed and integrated in the light transport model as LUTs. It is interesting to note that our model could be easily extended to the simulation of crystal arrays and the study of light spread between crystals.

A realistic model of light transport in scintillators based on a simple 3D characterization of crystal surfaces may have numerous potential applications in the field of nuclear medicine, particularly in the development of PET detectors. One motivation behind this work is to be able to model DOI-encoding PET detectors based on phosphor-coated crystals (Du *et al* 2009). Simulations would greatly help to understand the importance of different processes such as the effect of the surface treatment on the light conversion by the phosphor and the light collection. Further potential applications include other DOI-encoding and TOF-PET detectors as well as light guide design. With a proper model of the light transport in a scintillator, it becomes possible to study the light divergence at the exit face of the crystal. This has been studied in the past but is not trivial to measure (Haak *et al* 1997). The light angular distribution may then be used to enhance light collection and the coupling of the crystals to the photodetector. Finally, one advantage of this approach is that it is fully compatible with existing simulation toolkits such as GATE. Next steps include the implementation of our code in GATE together with a database containing different surface sample properties, and possible future implementation in ZEMAX.

Acknowledgments

This work was funded in part by grant DE-FG02-08ER85158 from the Department of Energy and by NIH grant CA134632. The authors want to thank the UC Davis Spectral Imaging Facility, particularly Alan Hicklin and Gang-Yu Liu for the AFM measurements.

References

Agostinelli S *et al* 2003 GEANT4—a simulation toolkit *Nucl. Instrum. Methods Phys. Res.* A **506** 250–303

Bauer F, Corbeil J, Schmand M and Henseler D 2009 Measurements and ray-tracing simulations of light spread in LSO crystals *IEEE Trans. Nucl. Sci.* **56** 2566–73

Bea J, Gadea A, Garcia-Raffi L M, Rico J, Rubio B and Tain J L 1994 Simulation of light collection in scintillators with rough surfaces *Nucl. Instrum. Methods Phys. Res.* A **350** 184–91

Cayouette F, Laurendeau D and Moisan C 2003 *DETECT2000: An improved Monte-Carlo Simulator for the Computer Aided Design of Photon Sensing Devices* ed R A Lessard *et al* (Quebec City, Canada: SPIE) pp 69–76

Du H, Yang Y, Glodo J, Wu Y, Shah K and Cherry S R 2009 Continuous depth-of-interaction encoding using phosphor-coated scintillators *Phys. Med. Biol.* **54** 1757–71

Gentit F-X 2002 Litrani: a general purpose Monte-Carlo program simulating light propagation in isotropic or anisotropic media *Nucl. Instrum. Methods Phys. Res.* A **486** 35–9

Haak G M, Christensen N L and Hammer B E 1997 Experimental studies on the angular distribution of scintillation light from small BGO crystals *Nucl. Instrum. Methods Phys. Res.* A **390** 191–7

Huber J S, Moses W W, Andreaco M S, Loope M, Melcher C L and Nutt R 1999 Geometry and surface treatment dependence of the light collection from LSO crystals *Nucl. Instrum. Methods Phys. Res.* A **437** 374–80

Jan S *et al* 2004 GATE: a simulation toolkit for PET and SPECT *Phys. Med. Biol.* **49** 4543

Janecek M and Moses W W 2009 Measuring light reflectance of BGO crystal surfaces *IEEE Trans. Nucl. Sci.* **55** 2443–9

Janecek M and Moses W W 2010 Simulating scintillator light collection using measured optical reflectance *IEEE Trans. Nucl. Sci.* **57** 964–70

Knoll G F, Knoll T F and Henderson T M 1988 Light collection in scintillation detector composites for neutron detection *IEEE Trans. Nucl. Sci.* **35** 872–5

Levin A and Moisan C 1996 A more physical approach to model the surface treatment of scintillation counters and its implementation into detect *IEEE Nuclear Science Symp. Conf. Record* pp 702–6

Melcher C L and Schweitzer J S 1992 Cerium-doped lutetium oxyorthosilicate—a fast, efficient new scintillator *IEEE Trans. Nucl. Sci.* **39** 502–5

Miyaoka R S, Lewellen T K, Yu H and McDaniel D L 1998 Design of a depth of interaction (DOI) PET detector module *IEEE Trans. Nucl. Sci.* **45** 1069–73

Moses W W and Derenzo S E 1994 Design studies for a PET detector module using a PIN photodiode to measure depth of interaction *IEEE Trans. Nucl. Sci.* **41** 1441–5

Moszynski M, Kapusta M, Mayhugh M, Wolski D and Flyckt S O 1997 Absolute light output of scintillators *IEEE Trans. Nucl. Sci.* **44** 1052–61

Nayar S K, Ikeuchi K and Kanade T 1991 Surface reflection: physical and geometrical perspectives *IEEE Trans. Pattern Anal. Mach. Intell.* **13** 611–34

Rothfuss H, Casey M, Conti M, Doshi N, Eriksson L and Schmand M 2004 Monte Carlo simulation study of LSO crystals *IEEE Trans. Nucl. Sci.* **51** 770–4

Shao Y, Meadors K, Silverman R W, Farrell R, Cirignano L, Grazioso R, Shah K S and Cherry S R 2002 Dual apd array readout of LSO crystals: optimization of crystal surface treatment *IEEE Trans. Nucl. Sci.* **49** 649–54

Slates R, Chatziioannou A, Fehlberg B, Taekyeung L and Cherry S 2000 Chemical polishing of LSO crystals to increase light output *IEEE Trans. Nucl. Sci.* **47** 1018–23

Spanoudaki V C and Levin C S 2011 Investigating the temporal resolution limits of scintillation detection from pixellated elements: comparison between experiment and simulation *Phys. Med. Biol.* **56** 735

van der Laan D J, Schaart D R, Maas M C, Beekman F J, Bruyndonckx P and van Eijk C W E 2010 Optical simulation of monolithic scintillator detectors using GATE/GEANT44 *Phys. Med. Biol.* **55** 1659

Yang Y, Dokhale P A, Silverman R W, Shah K S, McClish M A, Farrell R, Entine G and Cherry S R 2006 Depth of interaction resolution measurements for a high resolution PET detector using position sensitive avalanche photodiodes *Phys. Med. Biol.* **51** 2131–42

Yang Y, Wu Y and Cherry S R 2009 Investigation of depth of interaction encoding for a pixelated LSO array with a single multi-channel pmt *IEEE Trans. Nucl. Sci.* **56** 2594–9